Active one-particle microrheology of an unentangled polymer melt studied by molecular dynamics simulation

A. Kuhnhold* and W. Paul
Institut für Physik, Martin-Luther-Universität Halle-Wittenberg, 06099 Halle (Saale), Germany
(Received 16 December 2014; published 1 April 2015)

We present molecular dynamics simulations for active one-particle microrheology of an unentangled polymer melt. The tracer particle is forced to oscillate by an oscillating harmonic potential, which models an experiment using optical tweezers. The amplitude and phase shift of this oscillation are related to the complex shear modulus of the polymer melt. In the linear response regime at low frequencies, the active microrheology gives the same result as the passive microrheology, where the thermal motion of a tracer particle is related to the complex modulus. We expand the analysis to include full hydrodynamic effects instead of stationary Stokes friction only, and show that different approaches suggested in the literature lead to completely different results, and that none of them improves on the description using the stationary Stokes friction.

DOI: 10.1103/PhysRevE.91.042601 PACS number(s): 83.80.Sg, 83.10.Rs, 82.35.Np

I. INTRODUCTION

Microrheology is a method to study viscoelastic properties of materials by observing the motion of micron-sized tracer particles that are dispersed in the material. This method is therefore only applicable for soft matter but is becoming the method of choice for studying small probes, e.g., biological cells or small amounts of synthesized materials. The cornerstone for the development of microrheology was set by Mason and Weitz almost two decades ago [1]. They showed that the thermal motion of suspended particles can be related to the linear viscoelastic properties of the host material by assuming a generalized Stokes-Einstein relation (GSER). From then on, theory and experiments were extended [2–13]; one extension is active microrheology, where the forced motion of a tracer particle is studied instead of its thermal motion [14–21]. The force is applied in a pulsed, constant, or oscillating way, depending on the aim of the study, and the results of these procedures can be different.

With oscillatory active microrheology (OcAM) one can study the frequency dependence of the viscoelastic properties of the material and it is possible to either stay in the linear regime or to reach the nonlinear regime of the response. The corresponding experiments often use oscillating optical tweezers, which are mathematically described by harmonic potentials [14,18,21,22]. The tracer particles are trapped by the optical tweezers and follow their motion with a frequency-dependent amplitude and phase shift that depend on the surrounding material's properties. The relation to the complex shear modulus is derived by finding the connection between friction coefficient, ζ, and viscosity, η. In the steady limit, this is the Stokes equation $\zeta = \nu\pi\eta R$, with ν either 4 or 6, for slip or stick boundary conditions, respectively. Beyond this limit, one has to include other hydrodynamic effects, like shear waves and medium inertia. For a simple fluid and stick boundary conditions, those were already calculated by Stokes himself [23]: $\zeta = 6\pi\eta R(1+\tilde{\alpha}+\tilde{\alpha}^2/9)$, with $\tilde{\alpha} = R\sqrt{i\omega\rho/\eta}$ [24], and include the medium density ρ explicitly. This result is for purely viscous materials, and the generalization to viscoelastic materials can be done in two ways [25–27].

In Sec. II, we describe the model that is used to simulate the polymer melt and the tracer particle and explain how we model an oscillating optical tweezer. Then we show the derivation of the equations, which relate the amplitude and phase shift of the tracer to the storage and loss modulus of the surrounding medium in Sec. III. After this, we present our results in Sec. IV and compare them to our passive microrheological results. In Sec. V we discuss the inclusion of further hydrodynamic effects and compare results of two approaches. Finally, we conclude our findings in Sec. VI.

II. MODEL AND SIMULATION

Our polymer model is similar to the well-known bead-spring model of Kremer and Grest [28]: All pairs of monomers interact via a cut and shifted Lennard-Jones potential, where the shift function $U^{\mathrm{sh}}(r)$ makes sure that potential, force, and first derivative of force are equal to zero at the cutoff distance r_c [29,30]:

$$U_{mm}^{\mathrm{LJ}}(r) = \begin{cases} 4\epsilon_{mm}\left[\left(\frac{\sigma_{mm}}{r}\right)^{12} - \left(\frac{\sigma_{mm}}{r}\right)^{6}\right] + U_{mm}^{\mathrm{sh}}(r), & r \leqslant r_c \\ 0, & r > r_c \end{cases}. \quad (1)$$

This potential gives the energy, length, and time units of the system, $\epsilon_{mm} = 1$, $\sigma_{mm} = 1$, and $\tau = \frac{\sigma_{mm}}{\sqrt{\epsilon_{mm}/m}} = 1$, respectively, in which all values are measured. In addition, bonded monomers feel a finite-extensible-nonlinear-elastic (FENE) potential:

$$U_F(r) = -\frac{k}{2}R_F^2 \ln\left[1 - \left(\frac{r}{R_F}\right)^2\right], \quad (2)$$

with the force constant $k = 30$ and the maximum elongation $R_F = 1.5$.

The single tracer particle in the system also interacts via a Lennard-Jones potential with the monomers, but in addition

*anja.kuhnhold@physik.uni-halle.de

has a hard core of radius R_0:

$$U_{pm}^{\mathrm{LJ}}(r) = \begin{cases} 4\epsilon_{pm}\left[\left(\frac{\sigma_{pm}}{r-R_0}\right)^{12} - \left(\frac{\sigma_{pm}}{r-R_0}\right)^{6}\right] + U_{pm}^{\mathrm{sh}}(r), & r \leqslant r_c \\ 0, & r > r_c \end{cases}. \tag{3}$$

The length and energy scales of this potential are also set to unity, $\sigma_{pm} = 1$ and $\epsilon_{pm} = 1$. The cutoff distance for both Lennard-Jones interactions is set to $r_c = R_0 + 2 \cdot 2^{1/6}$, to include the repulsive and the attractive part of the interactions. For the hard-sphere radius we choose $R_0 = 2$ and set the tracer particle mass to $M = 25$.

The cubic simulation box with periodic boundary conditions in all dimensions contains 1572 polymer chains with 10 beads each. The average radius of gyration of those chains is $R_g = 1.5$. We apply a Nosé-Hoover thermostat on the polymer chains, not on the tracer, to simulate NVT ensembles. With this one avoids temperature drift, but still has local heating, as one has in experiments. The coupling time constant is $t_{NH} = 0.7$ and the simulation time step is $\delta t = 0.0035$. Well-equilibrated configurations are taken from former simulations [32]. We will show results for two temperatures $T = 0.5$ and $T = 1.06$. The box length for the lower temperature is 24.85, giving a monomer number density of $\rho = 1.03$. For the higher temperature it is 26.17, giving a monomer number density of $\rho = 0.88$. In all cases the box dimension is much larger than the tracer particle and the motion of the tracer has a small amplitude (cf. below), so that the influence of finite size effects is kept small.

An optical tweezer applies a force on dielectric particles, that can be modeled as harmonic in a region around its focus [25,26]. This makes the analysis of the results, but also the implementation in computer simulations, relatively easy: The oscillating optical tweezer is modeled as an oscillating external harmonic potential on the tracer particle:

$$U_{\mathrm{ot}}(r) = \frac{k_{\mathrm{ot}}}{2}(\mathbf{r} - \mathbf{r}_{\mathrm{ot}})^2 \tag{4}$$

$$\mathbf{r}_{\mathrm{ot}}(t) = [A\cos(\omega_{\mathrm{ot}}t), 0, 0]^T, \tag{5}$$

with the coupling constant k_{ot}, the oscillation amplitude A, and the frequency of the oscillation ω_{ot}. We choose the oscillations to be in the x direction and only consider the motion of the tracer in this direction for the microrheological analysis.

III. OSCILLATORY ACTIVE MICRORHEOLOGY

To derive the relation between the complex modulus of the material and the amplitude and phase shift of the tracer oscillation, one starts with a generalized Langevin equation in the direction of the oscillating trap:

$$M\ddot{x}(t) = F_R(t) - \int_0^t \zeta(t-t')\dot{x}(t')dt' - k_{\mathrm{ot}}[x(t) - A\cos(\omega_{\mathrm{ot}}t)], \tag{6}$$

which includes the particle inertia, a thermal, random force F_R, a friction force with memory kernel, and the oscillating harmonic trapping force as described above. Fourier transformation of both sides leads to

$$-M\omega^2\tilde{x}(\omega) = \tilde{F}_R(\omega) - \mathrm{i}\omega\tilde{\zeta}(\omega)\tilde{x}(\omega) - k_{\mathrm{ot}}\left\{\tilde{x}(\omega) - \frac{A}{2}[\delta(\omega-\omega_{\mathrm{ot}}) + \delta(\omega+\omega_{\mathrm{ot}})]\right\}, \tag{7}$$

with the δ distribution $\delta(\omega)$. The Gaussian distributed thermal force can be averaged out by ensemble averaging, and the friction coefficient is then

$$i\omega\tilde{\zeta}(\omega) = \frac{k_{\mathrm{ot}}A[\delta(\omega-\omega_{\mathrm{ot}}) + \delta(\omega+\omega_{\mathrm{ot}})]}{2\langle\tilde{x}(\omega)\rangle} + M\omega^2 - k_{\mathrm{ot}}. \tag{8}$$

Assuming a generalized Stokes relation between friction and viscosity [$\tilde{\zeta}(\omega) = \nu\pi\tilde{\eta}(\omega)R$], one gets the following results for the complex shear modulus of the material:

$$G^*(\omega) = \mathrm{i}\omega\tilde{\eta}(\omega) = \frac{\mathrm{i}\omega\tilde{\zeta}(\omega)}{\nu\pi R} = \frac{1}{\nu\pi R}\left\{\frac{k_{\mathrm{ot}}A[\delta(\omega-\omega_{\mathrm{ot}}) + \delta(\omega+\omega_{\mathrm{ot}})]}{2\langle\tilde{x}(\omega)\rangle}\right\} + \frac{1}{\nu\pi R}(M\omega^2 - k_{\mathrm{ot}}), \tag{9}$$

where ν is a parameter that determines the boundary conditions at the tracer particle surface, as discussed above. The effective hydrodynamic radius R is slightly larger than the hardcore radius of the tracer, because it is the radius, where the hydrodynamic boundary conditions have to be applied, and this is at the first maximum of the pair correlation function between tracer particle and monomers, which is at $R = R_0 + 1$.

The ensemble averaged motion of the tracer particle is expected to be oscillatory with the frequency of the external harmonic trap, the amplitude D, and the phase shift φ, which both depend on frequency:

$$\langle x(t)\rangle = D(\omega_{\mathrm{ot}})\cos[\omega_{\mathrm{ot}}t - \varphi(\omega_{\mathrm{ot}})]. \tag{10}$$

In Fourier space this is

$$\langle\tilde{x}(\omega)\rangle = \frac{D(\omega_{\mathrm{ot}})}{2}\{\cos[\varphi(\omega_{\mathrm{ot}})] - \mathrm{i}\sin[\varphi(\omega_{\mathrm{ot}})]\} \times [(\delta(\omega-\omega_{\mathrm{ot}}) + \delta(\omega+\omega_{\mathrm{ot}})]. \tag{11}$$

The storage and loss moduli are therefore calculated as [Eq. (11) in Eq. (9)]

$$G'(\omega_{\mathrm{ot}}) = \frac{1}{\nu\pi R}\left\{\frac{k_{\mathrm{ot}}A}{D(\omega_{\mathrm{ot}})}\cos[\varphi(\omega_{\mathrm{ot}})] + M\omega_{\mathrm{ot}}^2 - k_{\mathrm{ot}}\right\}, \tag{12}$$

$$G''(\omega_{\mathrm{ot}}) = \frac{1}{\nu\pi R}\frac{k_{\mathrm{ot}}A}{D(\omega_{\mathrm{ot}})}\sin[\varphi(\omega_{\mathrm{ot}})]. \tag{13}$$

IV. RESULTS

The amplitude of the external harmonic potential oscillation is set to $A = 0.1$. This seems to be rather small compared to the tracer particle radius of $R_0 = 2$ but is large enough to give reasonable results, as will be shown later. Furthermore, this amplitude cannot be much larger, because a combination of high frequency and large amplitude leads to numerical instabilities in the simulation due to excluded volume effects.

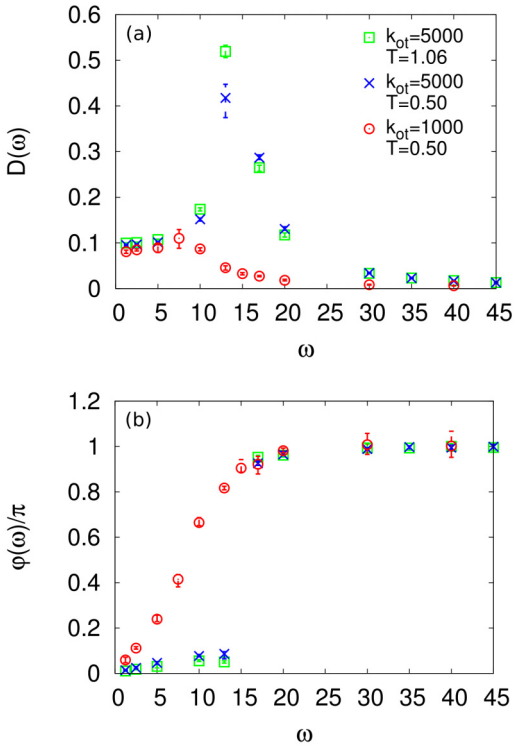

FIG. 1. (Color online) Amplitude (top) and phase shift (bottom) of the forced oscillation of a tracer particle with size $R_0 = 2$ at two different coupling constants and two different temperatures as indicated. The amplitude of the external potential oscillations is $A = 0.1$. Error bars show maximal and minimal values from subsets of oscillations.

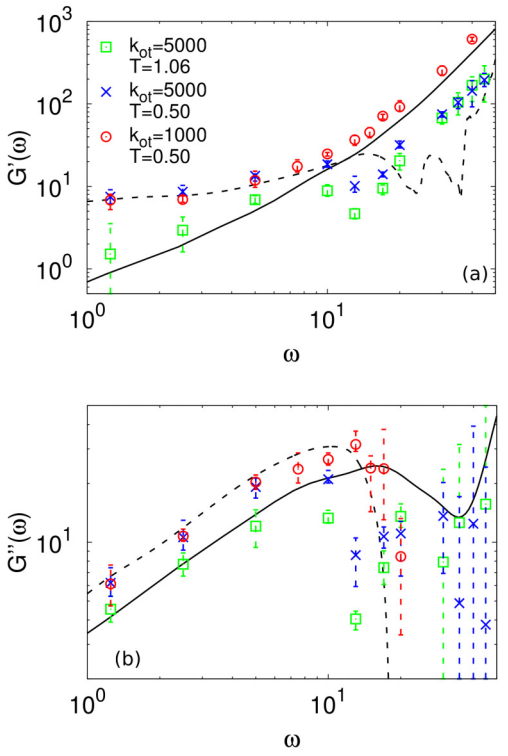

FIG. 2. (Color online) Storage (top) and loss modulus (bottom) derived with oscillatory active one-particle microrheology based on the amplitude and phase shift of the forced oscillation of a tracer particle with size $R_0 = 2$ at two different coupling constants and two different temperatures as indicated. The amplitude of the external potential oscillations is $A = 0.1$. The lines show the results from passive microrheology for the two temperatures $T = 1.06$ (solid) and $T = 0.50$ (dashed). Error bars show maximal and minimal values from subsets of oscillations.

We will discuss results for coupling constants between the external harmonic potential and the tracer particle of $k_{\rm ot} = 5000$ and $k_{\rm ot} = 1000$ and temperatures $T = 1.06$ and $T = 0.5$; the glass transition temperature of the model polymer melt is at $T_g = 0.41$ [31]. The amplitude and the phase shift of the forced oscillation of the tracer are shown in Fig. 1. At small frequencies, the amplitude is the same as the excitation amplitude and the phase shift tends to zero, because the tracer can follow the motion of the harmonic trap easily. At large frequencies, the amplitude tends to zero and the phase shift is π, because the harmonic trap moves too fast to be followed by the tracer. In between one finds characteristic resonance phenomena: (strong) increase of the amplitude and phase shift of $\pi/2$, which is either smoothly reached (strong damping) or via a jump (weak damping). Structure and mobility of the environment influence the resonance frequency and the damping of the oscillator. For the higher coupling strength, at both temperatures the environment effect is weak compared to the oscillator force and a sharp transition with a large resonance amplitude occurs. Upon reducing the coupling strength (or decreasing the temperature), the damping by the environment gets stronger and the motion can become overdamped. This is the case for $k_{\rm ot} = 1000$ and $T = 0.5$.

The storage and loss moduli are calculated from the amplitude and phase shift via Eqs. (12) and (13). The result is shown in Fig. 2. The lines are the moduli from passive microrheology, which we also studied for this system [32]. For frequencies $\omega < 10$, we find a good agreement between the active and the passive microrheology for both temperatures and both coupling constants. This means that we are in the linear response regime for $\omega < 10$, which is the only regime measurable with passive microrheology. At higher frequencies, the passive microrheology results are not reliable anymore, especially at low temperatures [32]. Here, the active microrheology reveals an increasing storage modulus coming from the inertia of the tracer $M\omega^2$, but an unsystematic result for the loss modulus with large error bars, because both $\sin[\varphi(\omega)]$ and $D(\omega)$ are getting small. The resonance is translated to a minimum in both storage and loss modulus but is hard to see for the low coupling case.

V. INCLUSION OF HYDRODYNAMIC EFFECTS BEYOND THE STATIONARY APPROXIMATION

In recent years, the importance of including hydrodynamic effects beyond the simple Stokes friction was stressed in the literature [33–37]. We did not find an improvement of our results in the passive microrheology of the studied system upon including these effects [32], but their influence on active microrheology has not yet been discussed in detail.

There are two approaches suggested in the literature to include complete hydrodynamic effects into the calculations.

They lead to different results, as will be shown in this paragraph. Both start with the solution of the Navier-Stokes equation for the nonstationary motion of a spherical particle moving in an incompressible Newtonian fluid (i.e., $\eta = \text{const.}$) with nonslip boundary conditions at its surface. The full friction coefficient reads [23,37]

$$\zeta(\omega) = 6\pi\eta R[1 + \tilde{\alpha}(\omega) + \tilde{\alpha}(\omega)^2/9], \tag{14}$$

$$\tilde{\alpha} = R\sqrt{i\omega\rho/\eta} \qquad [24], \tag{15}$$

where ρ is the fluid density. The complex shear modulus of a viscoelastic fluid is defined as $G^*(\omega) = i\omega\tilde{\eta}(\omega)$, where $\tilde{\eta}(\omega)$ is a frequency-dependent complex viscosity. The question now is, how the η in the Navier-Stokes solution, Eq. (14), relates to this complex viscosity. At this point, two different approaches are followed. In the first one, η is taken as the real part of $\tilde{\eta}(\omega) = \eta_m(\omega) - \mathrm{i}k_m(\omega)/(\omega\nu\pi R)$, where k_m then describes the elastic part of the response. In the second one, η is directly taken as the complex viscosity $\tilde{\eta}(\omega)$. Common to both approaches is the assumption that for a frequency-dependent viscosity the above relation between friction on the solute and fluid properties remains valid and one just has to make the viscosity in this equation frequency dependent. Of course, this is no longer the solution of a suitably modified Navier-Stokes equation, which would need to incorporate memory effects. This is a generally followed approach; however, it is far away from being accurate as we will see.

When η in the friction coefficient, Eq. (14), is a real valued viscosity η_m one can decompose ζ in a real and an imaginary part, and by rearranging these terms in Eq. (7) one finds

$$\begin{aligned} -M^*\omega^2\tilde{x}(\omega) = \tilde{F}_R(\omega) &- \mathrm{i}\omega 6\pi\eta_m^*(\omega)R\tilde{x}(\omega) \\ &- k_{\mathrm{ot}}\left\{\tilde{x}(\omega) - \frac{A}{2}[\delta(\omega-\omega_{\mathrm{ot}}) \right. \\ &\left. + \delta(\omega+\omega_{\mathrm{ot}})]\right\}, \end{aligned} \tag{16}$$

with [25,26]

$$M^*(\omega) = M + \frac{2}{3}\pi R^3\rho + 3\pi R^2\sqrt{\frac{2\eta_m(\omega)\rho}{\omega}} \tag{17}$$

$$\eta_m^*(\omega) = \eta_m(\omega)\left[1 + \sqrt{\frac{R^2\rho\omega}{2\eta_m(\omega)}}\right]. \tag{18}$$

However, this result is for purely viscous fluids only and one has to add the elastic part explicitly:

$$\begin{aligned} -M^*\omega^2\tilde{x}(\omega) = \tilde{F}_R(\omega) &- \mathrm{i}\omega 6\pi\eta_m^*(\omega)R\tilde{x}(\omega) - k_m(\omega)\tilde{x}(\omega) \\ &- k_{\mathrm{ot}}\left\{\tilde{x}(\omega) - \frac{A}{2}[\delta(\omega-\omega_{\mathrm{ot}}) \right. \\ &\left. + \delta(\omega+\omega_{\mathrm{ot}})]\right\}. \end{aligned} \tag{19}$$

Considering the case of stationary Stokes friction first by setting $M^* = M$ and $\eta_m^* = \eta_m$ and inserting the solution, Eq. (11), one finds the amplitude and phase shift of the tracer particle to be

$$D(\omega) = \frac{k_{\mathrm{ot}}A}{\sqrt{[k_{\mathrm{ot}} + k_m(\omega) - M\omega^2]^2 + [\nu\pi\eta_m(\omega)R\omega]^2}}, \tag{20}$$

$$\varphi(\omega) = \arctan\frac{\nu\pi\eta_m(\omega)R\omega}{k_{\mathrm{ot}} + k_m(\omega) - M\omega^2}, \tag{21}$$

and the spring constant and viscosity of the medium are

$$k_m(\omega) = \frac{k_{\mathrm{ot}}A}{D(\omega)}\cos[\varphi(\omega)] + M\omega^2 - k_{\mathrm{ot}}, \tag{22}$$

$$\eta_m(\omega) = \frac{k_{\mathrm{ot}}A}{\nu\pi R\omega D(\omega)}\sin[\varphi(\omega)], \tag{23}$$

where we have omitted the index *ot* from the frequency. With $G^*(\omega) = i\omega\tilde{\eta}(\omega) = i\omega[\eta_m(\omega) - ik_m(\omega)/(\omega\nu\pi R)]$ one rederives Eqs. (12) and (13).

For the complete Stokes friction one has to replace η_m and M in Eqs. (22) and (23) by η_m^* and M^*, respectively:

$$k_m(\omega) = \frac{k_{\mathrm{ot}}A}{D(\omega)}\cos[\varphi(\omega)] + M^*\omega^2 - k_{\mathrm{ot}}, \tag{24}$$

$$\eta_m^*(\omega) = \frac{k_{\mathrm{ot}}A}{\nu\pi R\omega D(\omega)}\sin[\varphi(\omega)]. \tag{25}$$

From Eqs. (25) and (18) one gets η_m and with that the loss modulus and from Eqs. (24) and (17) together with η_m one gets the storage modulus. With this, the storage and loss moduli with full hydrodynamic friction (index H) can be calculated from the storage and loss moduli with simple friction as

$$\begin{aligned} G'_{H,r}(\omega) = G'(\omega) &+ \left[-\frac{5}{6}R\rho \pm 3\sqrt{\frac{1}{4}R^2\rho^2 + \frac{2\rho G''(\omega)}{\omega^2}}\right] \\ &\times \frac{\omega^2 R}{6}, \end{aligned} \tag{26}$$

$$G''_{H,r}(\omega) = G''(\omega) + \left[\frac{1}{2}R\rho \mp \sqrt{\frac{1}{4}R^2\rho^2 + \frac{2\rho G''(\omega)}{\omega^2}}\right]\frac{\omega^2 R}{2}. \tag{27}$$

The two signs occur because one has to solve quadratic equations to get to the above results. The second index r stands for an ansatz with *real* viscosity, in contrast to the following.

The second way looks similar to the first one, but instead of the real viscosity η_m, the full hydrodynamic friction is written in dependence of a *complex* viscosity $\tilde{\eta}$:

$$\tilde{\zeta}(\omega) = 6\pi\tilde{\eta}(\omega)R(1 + \tilde{\alpha} + \tilde{\alpha}^2/9), \tag{28}$$

$$\tilde{\alpha} = R\sqrt{i\omega\rho/\tilde{\eta}(\omega)} \qquad [24]. \tag{29}$$

The definitions of the complex moduli $G^*_{H,c}(\omega) = \mathrm{i}\omega\tilde{\eta}(\omega)$ and $G^*(\omega) = \mathrm{i}\omega\tilde{\zeta}(\omega)/(6\pi R)$ then lead to [27]

$$\begin{aligned} G^*_{H,c}(\omega) = G^*(\omega) &- \frac{7}{18}R^2\rho\omega^2 \\ &\mp \frac{R^2\omega^2}{2}\sqrt{\frac{5}{9}\rho^2 - \frac{4\rho}{R^2\omega^2}G^*(\omega)}, \end{aligned} \tag{30}$$

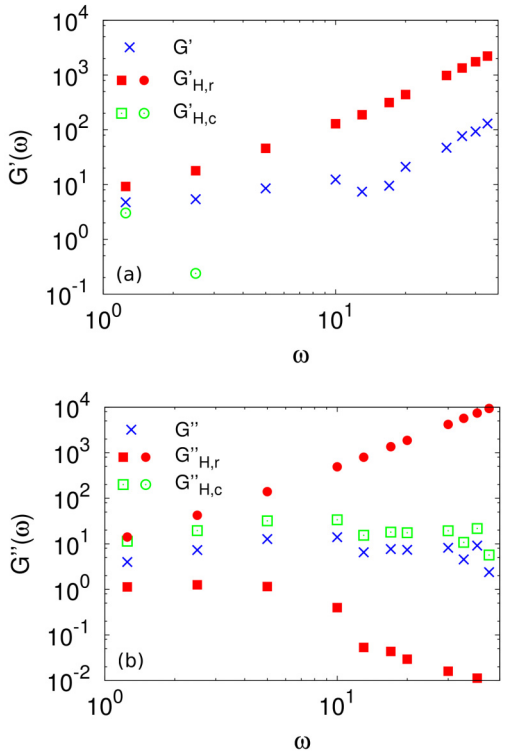

FIG. 3. (Color online) Storage (top) and loss modulus (bottom) derived with oscillatory active one-particle microrheology based on the amplitude and phase shift of the forced oscillation of a tracer particle with size $R_0 = 2$ at $k_{ot} = 5000$ and $T = 0.50$. The amplitude of the external potential oscillations is $A = 0.1$. Crosses: Evaluation using only the stationary Stokes friction [Eqs. (12) and (13)]. Filled symbols: Evaluation using full hydrodynamic friction with *real* viscosity [Eqs. (26) and (27)]. Open symbols: Evaluation using full hydrodynamic friction with *complex* viscosity [Eq. (30)]. Circles and squares are for upper and lower sign in the corresponding equations. Some results are negative and cannot be seen in this log-log plot.

which is obviously not the same as Eqs. (26) and (27). The second index c stands for an ansatz with *complex* viscosity.

The results for both versions and both signs are shown in Fig. 3, for one example ($k_{ot} = 5000$, $T = 0.50$). We do not show error bars anymore to keep the graphs clear, but keep in mind that they are large for the high-frequency loss modulus. For the storage modulus, one gets only one relevant result: the real ansatz and upper sign version. All other versions lead to negative values, except the two points from the complex ansatz and lower sign version included in the figure. For the loss modulus, one gets three relevant results: both real ansatz versions and the complex ansatz and upper sign version; all of them show different behaviors. The only version that gives qualitatively reasonable values for both moduli is the real ansatz with the upper sign. With this ansatz, the predicted storage modulus is higher than that resulting from stationary friction analysis, and the loss modulus is lower than the one obtained from it. In both cases, the agreement with the independently measured melt moduli [32] gets worse than for the simple analysis.

So far we used the results for nonslip boundary conditions because the solutions for the full friction coefficient are easy to handle. But actually our tracer model does not support nonslip conditions, since it has only one interaction site and therefore no tangential velocity. The full friction coefficient for slip boundary conditions is also known [37]:

$$\zeta(\omega) = 4\pi\eta R\left[1 + \frac{2\tilde{\alpha}(\omega)}{3+\tilde{\alpha}} + \tilde{\alpha}(\omega)^2/6\right], \tag{31}$$

$$\tilde{\alpha} = R\sqrt{i\omega\rho/\eta} \qquad [24]. \tag{32}$$

With this one can use the same approaches as described above. For the real ansatz one finds

$$M^*(\omega) = M + \frac{2}{3}\pi R^3\rho + \frac{24\pi R^2\sqrt{\rho\eta_m(\omega)/2\omega}}{9 + \rho\omega R^2/\eta_m(\omega) + 6R\sqrt{\rho\omega/2\eta_m(\omega)}}, \tag{33}$$

$$\eta_m^*(\omega) = \eta_m(\omega) \times\left[1 + \frac{6R\sqrt{\rho\omega/2\eta_m(\omega)} + 2R^2\rho\omega/\eta_m(\omega)}{9 + \rho\omega R^2/\eta_m(\omega) + 6R\sqrt{\rho\omega/2\eta_m(\omega)}}\right]. \tag{34}$$

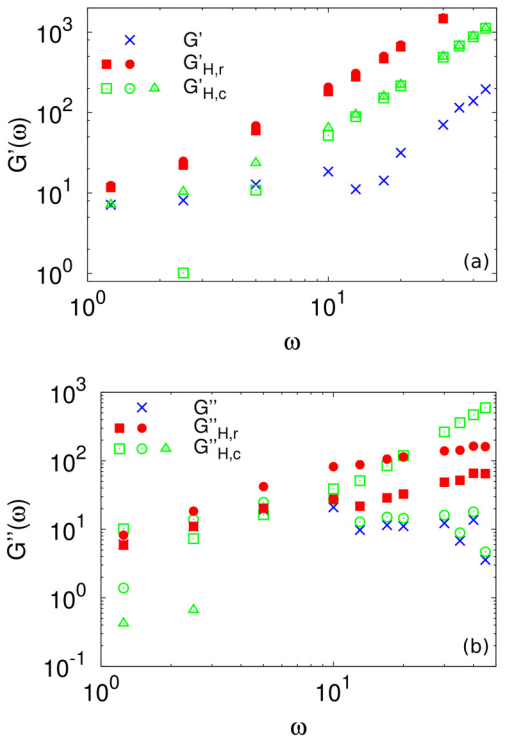

FIG. 4. (Color online) Storage (top) and loss modulus (bottom) derived with oscillatory active one-particle microrheology based on the amplitude and phase shift of the forced oscillation of a tracer particle with size $R_0 = 2$ at $k_{ot} = 5000$ and $T = 0.50$. The amplitude of the external potential oscillations is $A = 0.1$. Crosses: Evaluation using only the stationary Stokes friction [Eqs. (12) and (13)]. Filled symbols: Evaluation using full hydrodynamic friction with *real* viscosity. Open symbols: Evaluation using full hydrodynamic friction with *complex* viscosity. Circles, squares, and triangles are different solutions of the corresponding equations. Some results are negative and cannot be seen in this log-log plot.

Again, from Eqs. (25) and (34) one gets η_m and with that the loss modulus, and from Eqs. (24) and (33) together with η_m one gets the storage modulus.

For the complex ansatz one has to solve Eq. (31) with $\eta \to \tilde{\eta}(\omega)$ for the latter. This gives three solutions in contrast to the two solutions for nonslip conditions.

The results for the different approaches for slip boundary conditions are shown in Fig. 4. Again we find totally different results for the two approaches. All results for real-valued viscosities and also most of the results for complex-valued viscosities "correct" the moduli to higher values. Some versions are similar to the corresponding nonslip version (Fig. 3), but most of them are rather different. At the end we cannot state which approach, which solution, and which boundary condition is the correct one. The physics tells us only that the moduli have to be positive, that the storage modulus goes with ω^2 for high frequencies because of the tracer's inertia, and that the loss modulus must approach zero for high frequencies; which excludes only some of the possible solutions.

VI. CONCLUSION

In this publication, we discussed a simulation of oscillatory active microrheology of an unentangled polymer melt, by studying forced oscillations of a tracer particle for two coupling strengths and two temperatures. Employing a generalized Stokes-Einstein relation based on stationary Stokes friction and focusing on low frequencies, we found a very good agreement of these results with results from passive one-particle microrheology, showing the equivalence of both methods in the linear response regime. At high frequencies, the storage modulus is mainly governed by the inertia of the tracer particle and the particle motion decouples from the melt moduli.

Following recent discussions in the literature about including effects beyond the stationary Stokes friction, we showed two approaches to implement these; one using a real valued viscosity and one using a complex valued viscosity. In addition we evaluated the results for nonslip and slip boundary conditions. All lead to drastically different predictions for the frequency-dependent moduli, but none of these give a coherently reasonable representation of the actual moduli of the polymer melt, let alone an improvement compared to the approach based on the stationary Stokes friction. In view of the low number of publications using those approaches, it becomes clear that this topic has to be investigated further.

ACKNOWLEDGMENT

We thank the German Science Foundation for funding through SFB/TR 102.

[1] T. G. Mason and D. A. Weitz, Phys. Rev. Lett. **74**, 1250 (1995); T. G. Mason, K. Ganesan, J. H. van Zanten, D. Wirtz, and S. C. Kuo, *ibid.* **79**, 3282 (1997).
[2] T. G. Mason, Rheol. Acta **39**, 371 (2000).
[3] T. M. Squires and T. G. Mason, Annu. Rev. Fluid. Mech. **42**, 413 (2010).
[4] K. M. Addas, C. F. Schmidt, and J. X. Tang, Phys. Rev. E **70**, 021503 (2004).
[5] S. Yamada, D. Wirtz, and S. C. Kuo, Biophys. J. **78**, 1736 (2000)
[6] T.-H. Fan, J. K. G. Dhont, and R. Tuinier, Phys. Rev. E **75**, 011803 (2007); T.-H. Fan, B. Xie, and R. Tuinier, *ibid.* **76**, 051405 (2007).
[7] L.-H. Cai, S. Panyukov, and M. Rubinstein, Macromolecules **44**, 7853 (2011).
[8] S. A. Egorov, J. Chem. Phys. **134**, 084903 (2011).
[9] Q. Lu and M. J. Solomon, Phys. Rev. E **66**, 061504 (2002).
[10] S. Toyabe and M. Sano, Phys. Rev. E **77**, 041403 (2008).
[11] J. Sprakel, J. van der Gucht, M. A. Cohen Stuart, N. A. M. Besseling, Phys. Rev. Lett. **99**, 208301 (2007).
[12] H. Guo, G. Bourret, R. B. Lennox, M. Sutton, J. L. Harden, and R. L. Leheny, Phys. Rev. Lett. **109**, 055901 (2012).
[13] Y. Li, M. Kröger, and W. K. Liu, Phys. Rev. Lett. **109**, 118001 (2012).
[14] R. R. Brau, J. M. Ferrer, H. Lee, C. E. Castro, B. K. Tam, P. B. Tarsa, P. Matsudaira, M. C. Boyce, R. D. Kamm, and M. J. Lang, J. Opt. A: Pure Appl. Opt. **9**, S103 (2007); H. Lee, J. M. Ferrer, F. Nakamura, M. J. Lang, and R. D. Kamm, Acta Biomater. **6**, 1207 (2010).
[15] I. Gazuz, A. M. Puertas, Th. Voigtmann, M. Fuchs, Phys. Rev. Lett. **102**, 248302 (2009); M. V. Gnann, I. Gazuz, A. M. Puertas, M. Fuchs, Th. Voigtmann, Soft Matter **7**, 1390 (2011).
[16] I. C. Carpen and J. F. Brady, J. Rheol. **49**, 1483 (2005); A. S. Khair and J. F. Brady, J. Fluid Mech. **557**, 73 (2006).
[17] L. G. Wilson, A. W. Harrison, A. B. Schofield, J. Arlt, and W. C. K. Poon, J. Phys. Chem. B **113**, 3806 (2009); L. G. Wilson and W. C. K. Poon, Phys. Chem. Chem. Phys. **13**, 10617 (2011).
[18] D. Mizuno, D. A. Head, F. C. MacKintosh, and C. F. Schmidt, Macromolecules **41**, 7194 (2008).
[19] D. Winter, J. Horbach, P. Virnau, and K. Binder, Phys. Rev. Lett. **108**, 028303 (2012); Ch. J. Harrer, D. Winter, J. Horbach, M. Fuchs, Th. Voigtmann, J. Phys.: Condens. Matter **24**, 464105 (2012).
[20] T. M. Squires, Langmuir **24**, 1147 (2008); A. S. Khair and T. M. Squires, Phys. Rev. Lett. **105**, 156001 (2010).
[21] I. Sriram and E. M. Furst, J. Rheol. **53**, 357 (2009); I. Sriram, A. Meyer, and E. M. Furst, Phys. Fluids **22**, 062003 (2010).
[22] C. Chiang, M. Wei, Y. Chen, P. Yen, Y. Huang, J. Chen, O. Lavastre, H. Guillaume, D. Guillaume, and A. Chiou, Opt. Express **19**, 8847 (2011).
[23] G. G. Stokes, Trans. Cambridge Philos. Soc. **9**(part II), 8 (1851).
[24] $\tilde{\alpha}$ is often found as $\sqrt{-i\omega\rho/\eta}$. We use the other sign in the definition of the Fourier transformation, and therefore get $+i$.
[25] H. D. Ou-Yang, in *Colloid-Polymer Interactions: From Fundamentals to Practice* (Wiley, New York, 1999), pp. 385–405.
[26] M. T. Valentine, L. E. Dewalt, and H. D. Ou-Yang, J. Phys.: Condens. Matter **8**, 9477 (1996).
[27] M. Karim, S. C. Kohale, T. Indei, J. D. Schieber, and R. Khare, Phys. Rev. E **86**, 051501 (2012).
[28] K. Kremer and G. S. Grest, J. Chem. Phys. **92**, 5057 (1990).
[29] B. Hess, C. Kutzner, D. van der Spoel, and E. Lindahl, J. Chem. Theory Comp. **4**, 435 (2008).

[30] D. van der Spoel, E. Lindahl, B. Hess, A. R. van Buuren, E. Apol, P. J. Meulenhoff, D. P. Tieleman, A. L. T. M. Sijbers, K. A. Feenstra, R. van Drunen, and H. J. C. Berendsen, *Gromacs User Manual version 4.5.4*, www.gromacs.org (2010).

[31] K. Binder, J. Baschnagel, and W. Paul, Prog. Polym. Sci. **28**, 115 (2003).

[32] A. Kuhnhold and W. Paul, Phys. Rev. E **90**, 022602 (2014); J. Chem. Phys. **141**, 124907 (2014).

[33] B. U. Felderhof, Physica A **166**, 492 (1990); J. Chem. Phys. **123**, 044902 (2005); **123**, 184903 (2005).

[34] S. Jeney, B. Lukić, J. A. Kraus, T. Franosch, and L. Forró, Phys. Rev. Lett. **100**, 240604 (2008); T. Franosch, M. Grimm, M. Belushkhin. F. M. Mor, G. Foffi, L. Forró, and S. Jeney, Nature **478**, 85 (2011); M. Grimm, S. Jeney, and T. Franosch, Soft Matter **7**, 2076 (2011); M. Grimm, T. Franosch, and S. Jeney, Phys. Rev. E **86**, 021912 (2012).

[35] A. Córdoba, J. D. Schieber, and T. Indei, Phys. Fluids **24**, 073103 (2012).

[36] T. Indei, J. D. Schieber, A. Córdoba, and E. Pilyugina, Phys. Rev. E **85**, 021504 (2012); T. Indei, J. D. Schieber, and A. Córdoba, *ibid.* **85**, 041504 (2012).

[37] A. Erbas. R. Podgornik, R. R. Netz, Eur. Phys. J. E **32**, 147 (2010).